Journal of Photochemistry and Photobiology A: Chemistry 207 (2009) 102–108

Contents lists available at ScienceDirect

Journal of Photochemistry and Photobiology A: Chemistry

journal homepage: www.elsevier.com/locate/jphotochem

Linkage-structure dependences of the spectroscopic and photophysical properties of anthracene derivatives: Tri(9-anthryl)benzene and tri(9-anthryl)borane

Noboru Kitamura*, Eri Sakuda, Yoshie Iwahashi, Kiyoshi Tsuge[1], Yoichi Sasaki, Shoji Ishizaka

Department of Chemistry, Graduate School of Science, Hokkaido University, 060-0810 Sapporo, Japan

ARTICLE INFO

Article history:
Available online 20 January 2009

Dedicated to Professor Haruo Inoue on the occasion of his 60th birthday.

Keywords:
Tri(9-anthryl)benzene
Tri(9-anthryl)borane
Transition dipole moment
Fluorescence rate constant

ABSTRACT

The spectroscopic and photophysical properties of 1,3-di(9-anthryl)benzene (**DAB**), 1,3,5-tri(9-anthryl)benzene (**TAB**), and tri(9-anthryl)borane (**TABO**) in tetrahydrofuran were reported, together with those of 9-phenylanthracene (**MAB**). Although **MAB**, **DAB**, and **TAB** showed structured absorption spectra similar to the ^1L_a band of anthracene in the wavelength region of 300–400 nm, the molar absorption coefficient at the maximum wavelength of **TAB** was as large as ~4.2 as compared with that of **MAB**. Detailed analysis of the absorption data indicated that the absorption transition moment of **MAB**, **DAB**, or **TAB** was 3.3, 4.3, or 6.4 *D*, respectively. The large absorption transition moment of **TAB** was discussed on the basis of the electron density distributions in the highest-energy occupied and lowest-energy unoccupied molecular orbitals. In contrast to **TAB**, **TABO** exhibited characteristic broad and structureless absorption and fluorescence spectra. The large differences in the spectroscopic and photophysical properties between **TAB** and **TABO** were discussed in terms of the effects of the chemical structure of the terminal unit connecting three anthryl groups.

1. Introduction

Spectroscopic and photophysical properties of anthracene derivatives have been studied extensively during the past decades, in particular, those of 9- and 9,10-substituted anthracenes [1–3]. Among them, some derivatives show quite unique spectroscopic and photophysical characteristics. The representative example is 9,9′-bianthryl, and the compound shows broad and red-shifted fluorescence in the wavelength (λ) region of 370–600 nm. The fluorescence from 9,9′-bianthryl is different totally from that of anthracene and has been assigned to intramolecular charge transfer (CT) fluorescence [4]. It is also known that an introduction of an N,N-dimethylanilino group at the 9-position of anthracene (i.e., 4-(9-anthryl)-N,N-dimethylaniline) gives rise to the intramolecular CT-excited state, showing the fluorescence from both locally and CT-excited states in a polar medium [5]. Although the CT-excited state of 4-(9-anthryl)-N,N-dimethylaniline is readily understood by the presence of electron-donating (N,N-dimethylanilino group) and electron-accepting groups (anthryl group) in the molecule, CT nature in the excited state of 9,9′-bianthryl possessing two identical halves is quite interesting and, therefore, has been studied both experimentally and theoretically [4]. The unique spectroscopic and photophysical properties of 9,9′-bianthryl also suggest that those of multi-anthryl-chromophore compounds are very interesting.

As a new class of 9-substituted anthracene, synthesis and spectroscopic properties of 1,3,5-tri(9-anthryl)benzene (**TAB**) and tri(9-anthryl)borane (**TABO**) were reported recently by Suzuki et al. [6] and Yamaguchi et al. [7], respectively. As the structures are shown in Scheme 1, three anthryl groups are linked at the 1,3,5-positions of a benzene ring in **TAB** and those in **TABO** are connected directly with a boron atom. Molecular orbital (MO) calculations predict that both compounds possess propeller-like structures as shown in Scheme 1. In the case of **TABO**, in practice, the X-ray crystal structure analysis by Yamaguchi et al. [7a] and our research group [8] have demonstrated that the three carbon–boron bonds are in a planar configuration and the dihedral angle between the central boron and anthryl planes is ca. 53°. Similarly, our MO calculations indicate that the dihedral angle between the anthryl and central benzene planes in **TAB** is ca. 68° in average.

In addition to such structural characteristics of the compounds, **TABO** exhibits quite unique spectroscopic properties [7–10], showing a broad and intense absorption band at around 470 nm in addition to a structured anthracene-like band in 330–380 nm. In a dilute solution, furthermore, **TABO** exhibits broad and structureless fluorescence in 480–650 nm, which is different essentially from the monomer fluorescence of anthracene. Our spectroscopic

* Corresponding author. Tel.: +81 11 706 2697; fax: +81 11 706 4630.
E-mail address: kitamura@sci.hokudai.ac.jp (N. Kitamura).
[1] Present address: Department of Chemistry, Graduate School of Science, Osaka University, Toyonaka, 560-0043 Osaka, Japan.

1010-6030/$ – see front matter © 2009 Elsevier B.V. All rights reserved.
doi:10.1016/j.jphotochem.2009.01.003

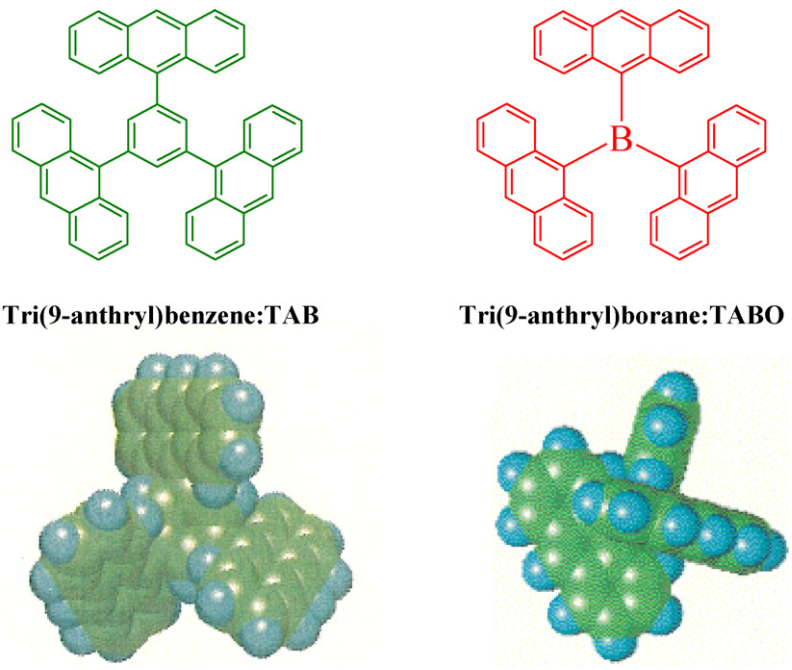

Scheme 1. Molecular structures of 1,3,5-tri(9-anthryl)benzene (**TAB**) and tri(9-anthryl)borane (**TABO**).

and photophysical studies indicate that the absorption and fluorescence characteristics of **TABO** mentioned above are explained by the intramolecular CT transition between the π-orbital of the anthryl group and the p-orbital of the boron atom [9]. Recent experimental and theoretical works by Wang et al. also support such conclusions [10]. On the other hand, although the absorption and fluorescence maximum wavelengths of **TAB** in a solid phase have been reported to be 396 and 456 nm, respectively [6], the crystal structure and spectroscopic/photophysical properties of **TAB** have not been reported yet. The spectroscopic and photophysical properties of multi-anthryl-chromophore compounds are interesting as mentioned above and such a type of compounds has been received current attention as light emitting materials [11], fluorescence sensors [12], and so forth [13]. Therefore, the spectroscopic and photophysical properties of **TAB** are worth studying and comparing with those of other anthracene derivatives.

In the present study, we focused our experiments on elucidating how the chemical structure connecting three anthryl groups influenced the spectroscopic and photophysical properties of the molecule: **TAB** (benzene ring) vs. **TABO** (boron atom). For this purpose, we synthesized **TAB** and conducted X-ray crystal structure analysis. To pursue such a study, furthermore, 9-phenylanthracene (**MAB**) and 1,3-di(9-anthryl)benzene (**DAB**) were employed as reference compounds for **TAB**. In the present paper, we report the spectroscopic and photophysical properties of **MAB**, **DAB**, **TAB**, and **TABO**. On the basis of such an experimental study, we show that the benzene ring or boron atom connecting three anthryl groups in **TAB** or **TABO**, respectively, governs essentially the spectroscopic and photophysical characteristics of the derivative.

2. Experimental

2.1. Preparation of DAB and TAB

DAB and **TAB** were prepared by a palladium-catalyzed cross-coupling reaction between 1,3,5-tribromobenzene and 9-anthracene boronic acid as described below [6,14].

Into a toluene (40 mL)–ethanol (20 mL) solution of 1,3,5-tribromobenzene (1.0 g, 3.2 mmol, Wako Pure Chemicals Co., Ltd.) and 9-anthracene boronic acid (4.3 g, 19 mmol) [6,14a,14b] were added an aqueous Na_2CO_3 solution (2 mol/L, 97 mL) and tetrakis(triphenylphosphine)palladium(0) ($Pd(PPh_3)_4$, 0.55 g, 0.5 mmol, Tokyo Kasei Kogyo Ltd.) under N_2-gas atmosphere, and the mixture was refluxed for 5 h under stirring. After cooling, the mixture was extracted with chloroform and the organic layer dried over Na_2SO_4 was evaporated. The crude product was purified successively by column chromatography (silica gel, toluene:*n*-hexane = 1:3, v/v) and recrystallization from toluene: yield = 29% (colorless crystals). FD-MS *m*/*z* 606. Anal. (calcd.) for $C_{48}H_{30}$: C, 94.13 (95.01); H, 5.24 (4.98). ^{1}H NMR ($CDCl_3$, 270 MHz), δ (ppm): 7.48 (*dt*, 6H, *J* = 1.5 and 7.2 Hz), 7.54 (*dt*, 6H, *J* = 1.6 and 7.4 Hz), 7.75 (*s*, 3H), 8.05 (*dd*, 6H, *J* = 1.5 and 8.5 Hz), 8.18 (*dd*, 6H, *J* = 1.1 and 8.6 Hz), 8.50 (*s*, 3H).

In the course of synthetic experiments on **TAB**, **DAB** was also obtained by the following procedures. Into an ethylene glycol dimethyl ether (Kanto Chemical Industry Co., Ltd.) solution of 1,3,5-tribromobenzene (0.45 g, 1.5 mmol) and 9-anthracene boronic acid (2.0 g, 9 mmol) was added an aqueous ethanol solution (H_2O 25 mL/ethanol 20 mL) of $Ba(OH)_2$ (0.8 mol/L, Wako Pure Chemicals Co., Ltd.) under stirring. The mixture was deaerated by purging an N_2-gas stream for 20 min and refluxed for 78 h in the presence of $Pd(PPh_3)_4$ (0.60 g, 0.6 mmol). After adding 50 mL of water, the solution was extracted with CH_2Cl_2 (100 mL). The organic layer separated was washed with an aqueous NaCl solution and dried over $MgSO_4$. Evaporation of the solvent gave **DAB** with **TAB** being a minor product (~2%) as judged from FD-MS. The crude product was then washed successively with an ethyl acetate–diethyl ether mixture (1:1, v/v) and acetone, giving **DAB** with the yield of ~10% (colorless solid). FD-MS *m*/*z* 430. Anal. (calcd.) for $C_{34}H_{22}$: C, 92.74 (94.85); H, 5.16 (5.15). ^{1}H NMR ($CDCl_3$, 270 MHz) δ (ppm): 7.43 (*dt*, 4H, *J* = 2.1 and 7.2 Hz), 7.47 (*dt*, 4H, *J* = 2.0 and 7.1 Hz), 7.54 (*t*, 1H, *J* = 1.6 Hz), 7.62 (*dd*, 2H, *J* = 1.5 and 7.7 Hz), 7.80 (*t*, 1H, *J* = 7.5 Hz), 7.92 (*dd*, 4H, *J* = 2.3 and 8.2 Hz), 8.04 (*dd*, 4H, *J* = 2.2 and 8.6 Hz), 8.49 (*s*, 2H).

Although the elemental analyses of **TAB** and **DAB** did not necessarily agree with the calculated values as described above, we confirmed that the compounds were spectroscopically and photophysically pure as judged from ^{1}H NMR and absorption/fluorescence spectroscopies as described in the following sections.

2.2. Other chemicals

9-Phenylanthracene (**MAB**, Aldrich) was purified by recrystallization from toluene. Spectroscopic grade tetrahydrofuran (THF), toluene, and acetonitrile, purchased from Wako Pure Chemicals Co., Ltd., were used as supplied.

2.3. Spectroscopic and photophysical measurements

Absorption and corrected fluorescence spectra were recorded on a Hitachi U-3300 spectrophotometer and a Hitachi F-4500 spectrofluorometer, respectively. The fluorescence quantum yield (Φ^{f}) of a sample solution was determined by using a cyclohexane solution of 9,10-diphenylanthracene (**DPA**) as a standard ($\Phi^{f}_{ST} = 0.86$) [15]. For determination of the fluorescence quantum yield, the absorbance (A) of a sample solution at an excitation wavelength (338 nm) was set at ~0.02 and the refractive index correction was made according to Eq. (1):

$$\frac{\Phi^{f}}{\Phi^{f}_{ST}} = \frac{F}{F_{ST}} \times \frac{A_{ST}}{A} \times \frac{n^2_{ST}}{n^2} \quad (1)$$

where F and n represent the spectral integral in a wavenumber scale and the refractive index of a solvent, respectively. The subscript (ST) in Eq. (1) represents the value for **DPA**. Fluorescence lifetime measurements were conducted by using a picosecond single photon counting system reported previously: excitation wavelength = 400 nm [16]. For fluorescence spectroscopy, the sample solution was deaerated by purging an Ar-gas stream over 20 min prior to the experiments. All the measurements were conducted at 23 °C.

2.4. X-ray crystallography

The X-ray structural data of **TAB** were collected on Mercury CCD area detectors coupled with Rigaku AFC-8S and AFC-7R diffractometers, respectively, by using CrystaClear (Rigaku Co.) with graphite-monochromated Mo Kα radiation (0.7107 Å). The structures were solved with a Silicon Graphics O2 computer system by using teXsan, version 1.1 (Molecular Structure Co.). Full-matrix least-squares refinements were employed against F^2.

3. Results and discussion

3.1. X-ray crystal structure of TAB

Fig. 1 shows the crystal structure of **TAB** and, Tables 1 and 2 summarize the crystallographic data and selected bond distances, respectively. The X-ray crystal structure analysis demonstrates that two types of **TAB** are involved in the crystal, with the angle between the bridging benzene plane and each anthryl π plane being different: 86.8°, 88.4°, and 76.1° for Type-I; 78.8°, 85.3°, and 82.8° for Type-II. For both Type-I and -II, **TAB** possesses a propeller-like structure as predicted from the MO calculations as seen in Scheme 1 and Fig. 1. The dihedral angle between any of two anthryl π planes (center-to-center, ∠An–An) in **TAB** was ~120°, reflecting D_3 molecular symmetry. **TABO** with D_3 symmetry also possesses a propeller-like structure (see Scheme 1) and ∠An–An has been reported to be ~120° [7a]. Judging from the ∠An–An values, both **TAB** and **TABO** will not show an intramolecular π–π interaction between the anthryl groups. In the case of **TABO**, in practice, no intramolecular interaction has been observed as revealed by absorption and fluorescence spectroscopies in both solution and crystal phases [8,9].

TAB is structurally less crowded as compared with **TABO**. This is readily understood, since three anthryl groups in **TAB** are linked at the 1,3,5-positions of a benzene ring, while those in **TABO** are

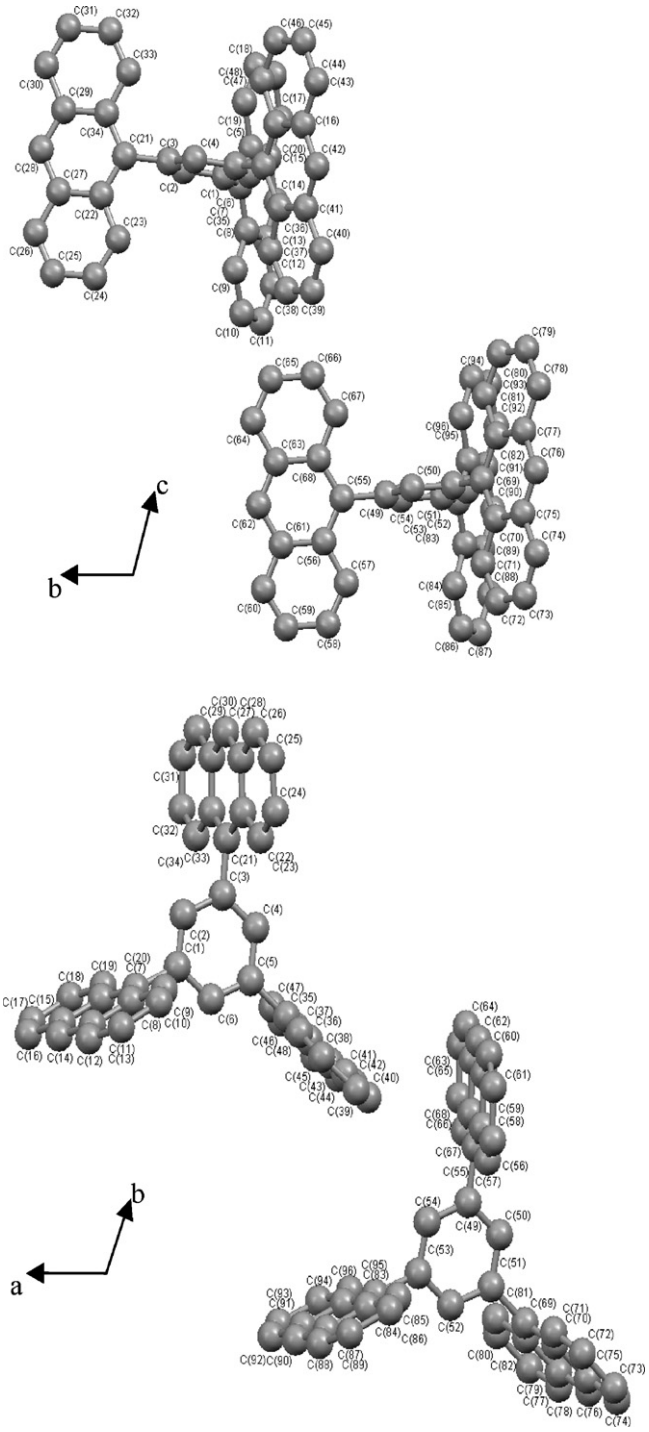

Fig. 1. Crystal structures of **TAB**.

connected directly with a boron atom. In practice, the bond length between the boron atom and carbon atom at the 9-position of the anthryl group (C–9) in **TABO** has been reported to be 1.58 Å [7a], while that between the center of the bridging benzene ring and C–9 in **TAB** is 2.88 Å. In the unit cell, two Type-II **TAB** molecules sit around one Type-I **TAB** with the distance between the Type-I and -II anthryl groups being 4.8 Å: see Fig. 1. Although this suggests a possibility of an intermolecular interaction between the anthryl groups in the crystalline phase, fluorescence spectroscopy experiments on **TAB** crystals have demonstrated that no intermolecular interaction participates between adjacent **TAB** molecules.

Table 1
The crystal structure of **TAB**.

Crystal-form	
Formula	$C_{108}H_{68}$
F.W.	1305.67
Size (mm)	0.54 × 0.50 × 0.25
T (K)	213.1
Cryst syst	Triclinic
Space group	P-1
Cell constant	
a (Å)	13.3566(11)
b (Å)	14.4993(11)
c (Å)	19.447(2)
α (°)	92.085(3)
β (°)	102.687(3)
γ (°)	101.158(3)
V (Å^3)	3592.5(5)
Z	1
ρ_{calc} (g/cm^3)	0.660
μ (cm^{-1})	0.403
λ (Mo Kα) (Å)	0.7107
*R*1%	0.0665
w*R*2%	0.1810

T, measured temperature; *Z*, formula units/cell; ρ_{calc}, calculated density; *μ*, linear absorption coefficient; λ, radiation wavelength $R1 = \sum ||F_o| - |F_c|| / \sum |F_o|$ $wR2 = \left[\sum (|F_o| - |F_c|)^2 / \sum w|F_o|^2\right]^{1/2}$.

Table 2
Selected bond distances (Å) of **TAB**.

Atom	Atom	Distance	Atom	Atom	Distance
C(1)	C(7)	1.492(3)	C(4)	C(55)	1.495(2)
C(3)	C(21)	1.497(2)	C(51)	C(69)	1.488(2)
C(5)	C(35)	1.492(2)	C(53)	C(83)	1.493(3)
C(1)	C(2)	1.389(2)	C(49)	C(50)	1.381(2)
C(2)	C(3)	1.392(3)	C(50)	C(51)	1.397(2)
C(3)	C(4)	1.384(2)	C(51)	C(52)	1.388(3)
C(4)	C(5)	1.396(2)	C(52)	C(53)	1.381(2)
C(5)	C(6)	1.388(3)	C(53)	C(54)	1.390(2)
C(1)	C(6)	1.384(2)	C(49)	C(54)	1.394(3)

3.2. Absorption characteristics of MAB, DAB, and TAB

Fig. 2 shows the absorption spectra of **MAB**, **DAB**, and **TAB** in THF, and the absorption parameters are summarized in Table 3. The three derivatives showed structured absorption spectra similar to that of anthracene (**An**) [1], while the absorption maximum wavelength (λ^a) was shifted to a longer wavelength by 9, 10, or 12 nm for **MAB**, **DAB**, or **TAB**, respectively, as compared with that of **An** (λ^a = 377 nm in THF). The similarities of the observed absorption spectrum of **MAB**, **DAB**, or **TAB** with the ^1L_a band of **An** indicate that the absorption transition dipole of each derivative directs along the short axis of the anthryl group [1]. The present data also demonstrate that the absorption spectrum of the derivative shows a sharp envelope in the longer-wavelength absorption edge. Therefore, no intramolecular interaction between the anthryl groups participates in the ground state of **TAB**, in good agreement with the prediction from the molecular structure in Fig. 1 and Scheme 1. Furthermore, although an introduction of a phenyl group at the 9-position of anthracene (i.e., **MAB**) gives rise to a spectral red shift from 377 (**An**) to 386 nm (**MAB**), that of one or two anthryl group(s) to **MAB** results in a 1 (**DAB**, 387 nm) or 3 nm spectral shift (**TAB**, 389 nm), respectively. Therefore, as long as the absorption spectral band shape and wavelength are concerned, large differences in the electronic structures are not confirmed between the three derivatives.

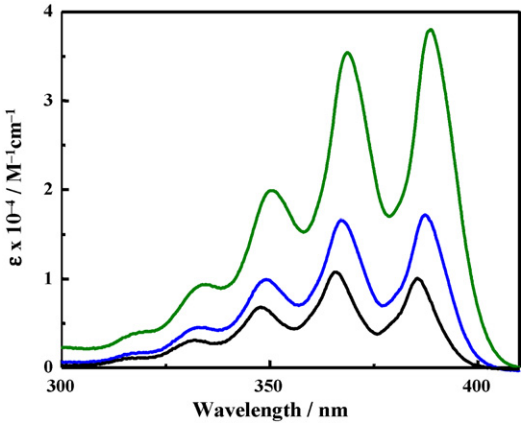

Fig. 2. Absorption spectra of **MAB** (black curve), **DAB** (blue curve), and **TAB** (green curve) in THF at room temperature. (For interpretation of the references to color in this figure legend, the reader is referred to the web version of the article.)

Table 3
Absorption parameters of the anthracene derivatives in THF.

	λ^a (nm)	$\varepsilon \times 10^{-4}$/M^{-1} cm^{-1} ($\varepsilon^{rel}$)	*f*	*μ* (Debye)
MAB	386	0.91(1.00)	0.13	3.3
DAB	387	1.7(1.87)	0.22	4.3
TAB	389	3.8(4.18)	0.50	6.4

On the other hand, the data in Fig. 2 and Table 3 demonstrate clearly that the molar absorption coefficient (*ε*) of the derivative at λ^a increases with the increase in the number of the anthryl group introduced to a benzene ring: *ε* = **MAB** < **DAB** < **TAB**. The *ε* value of **DAB** was almost two times larger (ε^{rel} = ∼1.9 in Table 3) than that of **MAB**, which was the reasonable consequence as the results of the two anthryl groups in **DAB**. In the case of **TAB**, however, an introduction of three anthryl groups to a benzene ring brought about a ∼4.2-fold increase in the *ε* value as compared with that of **MAB**, without any appreciable change in the spectral band shape between the two derivatives: see Fig. 2. As a rough approximation, an introduction of three anthryl groups to a benzene ring should give rise to a threefold increase in the *ε* value as compared with that of **MAB**. The large *ε* value of **TAB** is thus quite interesting and worth discussing in some more detail.

The dipole moment of a given absorption transition ($\tilde{\mu}$) can be evaluated by the absorption spectrum and the following equations [1]:

$$f = 4.39 \times 10^{-9} \int \varepsilon \, d\tilde{\nu} \tag{2}$$

$$\tilde{\mu} = \left[\frac{3he^2 f}{8\pi^2 m_e c \tilde{\nu}_0}\right]^{1/2} \tag{3}$$

where *f* represents the oscillator strength of an absorption transition. The integral in Eq. (2) is the spectral integral of a given absorption transition in a wavenumber ($\tilde{\nu}$) scale. In Eq. (3), *h*, *e*, m_e, *c*, and $\tilde{\nu}_0$ are the Planck's constant, the electron charge, the mass of an electron, the speed of light, and the absorption maximum energy, respectively. The absorption spectra of the derivatives in 300–420 nm ($\tilde{\nu}$ = 33, 300–23, 800 cm^{-1}) in Fig. 2 and Eqs. (2) and (3) demonstrated that the $\tilde{\mu}$ value of **MAB**, **DAB**, or **TAB** was 3.3 (*f* = 0.13), 4.3 (0.22), and 6.4 *D* (0.50), respectively. Despite the symmetrical structure of **TAB**, the compound possesses a relatively large $\tilde{\mu}$ value.

To understand such experimental results, we conducted molecular mechanics calculations (MM2). Fig. 3 shows graphical displays of the electron density distributions in the highest-energy occupied and lowest-energy unoccupied molecular orbitals (HOMO and LUMO, respectively) of each derivative. In the case of **MAB** or **DAB**, the electron density almost resides on the anthryl group(s) in both HOMO and LUMO, with the minor contribution of the density in

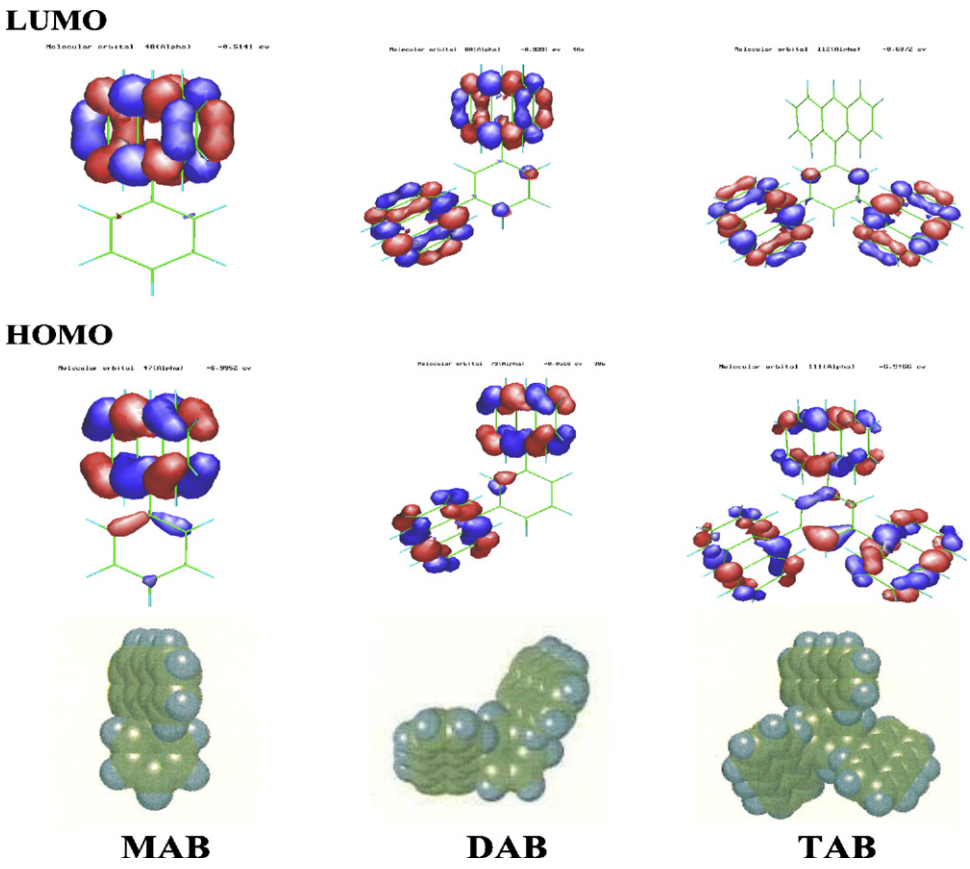

Fig. 3. Electron density distributions in the HOMO and LUMO of **MAB**, **DAB**, and **TAB**.

the bridging benzene ring. Similar electron density distributions in the HOMO and LUMO to those of **MAB** or **DAB** have been reported for several 9- and 9,10-substituted anthracenes [17]. In the case of **TAB**, the electron density in the HOMO distributes to both benzene ring and three anthryl groups, while the LUMO is best characterized by the large electron density in the two anthryl groups. This indicates that **TAB** should accompany a relatively large dipole moment change upon photoexcitation from the HOMO to LUMO, while this is not the case for **MAB** or **DAB**. The results agree very well with the larger $\tilde{\mu}$ and f values observed for **TAB** as compared with those of **MAB** and **DAB**. It has been reported that the dipole moment change ($\Delta\mu$) upon photoexcitation from the ground state (μ_g) to the excited state (μ_e: $\Delta\mu = \mu_e - \mu_g$) of 10-N,N-dimethylamino-9-cyanoanthracene as an intramolecular CT type compound is 5.4 D [17b]. The $\Delta\mu$ value of **TABO** possessing the CT-excited state has been also reported to be ~8.0 D [9]. Therefore, the $\tilde{\mu}$ value of **TAB** is as large as that of an intramolecular CT type anthracene derivative. Although the absorption spectral band shape of **TAB** is similar to that of **MAB** or **DAB**, **TAB** possesses the unique electronic structures, different from those of **MAB** or **DAB**.

3.3. Fluorescence characteristics of MAB, DAB, and TAB

Fig. 4 shows the fluorescence spectra of **MAB**, **DAB**, and **TAB** in THF and the fluorescence parameters are listed in Table 4. Reflecting the absorption spectral red shift in the sequence of **MAB** < **DAB** < **TAB**, the fluorescence maximum wavelength (λ^f) was also shifted to a longer wavelength in the same sequence without appreciable change in the spectral band shape. No intra/intermolecular interaction or excimer formation was observed for **TAB** in the concentration range of 4.9×10^{-6} to 6.9×10^{-5} mol/L, which was in good agreement with the predictions from the molecular structure in Fig. 1. Since the fluorescence spectra of the three compounds shown in Fig. 4 were observed under analogous experimental conditions (see also Section 2), the sequence of the fluorescence intensity almost corresponded to that of the fluorescence quantum yield (Φ^f): **MAB** (0.69) < **DAB** (0.71) < **TAB** (0.85). The Φ^f value of **TAB** was comparable to that of 9,10-diphenylanthracene (**DPA**, 0.86), while that of **MAB** was somewhat larger than the literature value: 0.49 (ethanol) [1]. Generally, the determination of Φ^f is erroneous with an uncertainty in ±10%. However, since the Φ^f value of **TAB** is comparable with that of **DPA** as mentioned above, the results in Fig. 4 demonstrate that **MAB** and **DAB** also show intense fluorescence.

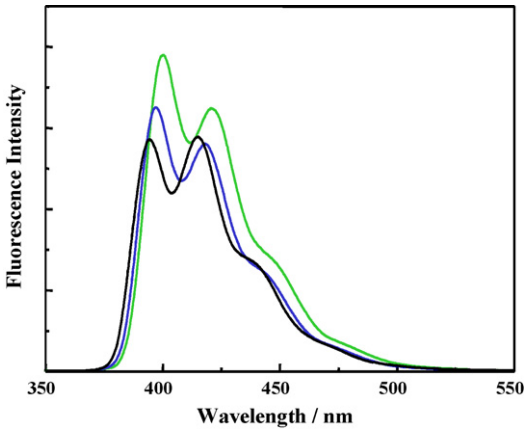

Fig. 4. Corrected fluorescence spectra of **MAB** (black curve), **DAB** (blue curve), and **TAB** (green curve) in deaerated THF at room temperature. The absorbance of the sample solution at the excitation wavelength (338 nm) was set at ~0.02. (For interpretation of the references to color in this figure legend, the reader is referred to the web version of the article.)

Table 4
Fluorescence parameters of the anthracene derivatives in THF.

	λ^f (nm)	Φ^f	τ^f (ns)	k_f ($\times 10^{-8}$ s^{-1})	k_f^0 ($\times 10^{-8}$ s^{-1})	k_{nr} ($\times 10^{-7}$ s^{-1})
MAB	394	0.69	7.1	0.97	0.61	4.4
DAB	397	0.71	6.6	1.1	1.0	4.4
TAB	400	0.85	6.8	1.3	2.3	2.2
TABO[a]	535	0.06	4.3	0.14	1.5	22

[a] Data compiled from Ref. [9a].

The emission from each derivative showed a single exponential decay with the lifetime of $\tau^f = 7.1$ ($\chi^2 = 1.13$, D.W. = 1.88), 6.6 (1.02, 2.01), or 6.8 ns (1.10, 1.92) for **MAB**, **DAB**, or **TAB**, respectively, where χ^2 and D.W. represent chi-squared and Durbin–Watson parameters for the fluorescence decay fitting, respectively. The fluorescence lifetime of **MAB** agrees very well with the literature value: 6.5 ns in cyclohexane [1].

On the basis of the Φ^f and τ^f values, we evaluated the fluorescence (k_f) and nonradiative decay rate constants (k_{nr}) of the derivative by the relation of $\Phi^f = k_f/(k_f + k_{nr}) = k_f\tau^f$, where $k_{nr} = (k_{ic} + k_{isc})$; k_{ic} and k_{isc} are the rate constants of internal conversion to the ground state and intersystem crossing to the excited triplet sate, respectively. Although there is no experimental evidence, we suppose that intersystem crossing to the excited triplet state will be the major nonradiative decay path from the excited singlet state of the derivative (i.e., $k_{isc} > k_{ic}$), similar to the most of the excited $\pi\pi^*$ singlet states of aromatic hydrocarbons [1]. The k_f and k_{nr} values calculated are included in Table 4. It is worth emphasizing that the k_f value of **MAB**, **DAB**, or **TAB** ($\sim 1 \times 10^8$ s^{-1}) is larger than k_{nr} ($(2–4) \times 10^7$ s^{-1}). Furthermore, the k_f value increases in the sequence of **MAB** < **DAB** < **TAB**, and this sequence agrees with that of the ε or Φ^f value. To discuss such experimental observations, we introduce the following Strickler–Berg equation:

$$k_f^0 = 3.0 \times 10^{-9} \tilde{\nu}_0^2 \int \varepsilon \, d\nu \quad (4)$$

where k_f^0 is the intrinsic fluorescence rate constant. On the basis of the absorption spectral data in Fig. 2 and Eq. (4), we calculated the k_f^0 value of the derivative. As the data are included in Table 4, the k_f^0 values of **MAB**, **DAB**, and **TAB** agree well with the observed k_f values, demonstrating that the nonradiative decay from the excited singlet state is a minor path as compared with the radiative process. Furthermore, the results indicate that both absorption and fluorescence transition probabilities of the derivative increase with the increase in the number of the anthryl group introduced to a benzene ring. In the case of **TAB**, in particular, the large ε value gave rise to intense fluorescence with $\Phi^f = 0.85$. Therefore, the characteristic electron density distributions in the HOMO and LUMO in Fig. 3 could be the origin of both absorption and fluorescence characteristics of **TAB**.

The results mentioned above suggest that 1,3,5-triarylbenzene, having HOMO–LUMO electron density distributions similar to those of **TAB** in Fig. 3, may also show intense fluorescence. Besides **TAB**, 1,3,5-tri(1-naphthyl)benzene, 1,3,5-tri(2-naphthyl)-benzene [14a], and 1,3,5-tri(1-pyrenyl)benzene [6] have been hitherto reported. Although detailed spectroscopic and photophysical studies on these compounds have not been reported, 1,3,5-tri(1-pyrenyl)benzene has been suggested to show more intense fluorescence than **TAB** [6]. The present results indicate that 1,3,5-triarylbenzene would be a possible candidate for an intense fluorescent material.

3.4. Spectroscopic and photophysical characteristics of TAB and TABO: a comparative study

The absorption and fluorescence spectra of **TABO** in THF (data taken from Ref. [9a]) are shown in Fig. 5, together with those of **TAB** for comparison. The absorption and fluorescence parameters of **TABO** are included in Tables 3 and 4, respectively. It is very clear from Fig. 5 that the absorption and fluorescence spectra of **TABO** are different from the relevant spectrum of **TAB**. **TABO** shows a broad and structureless absorption band at around 475 nm and a structured band in 330–400 nm. The structured absorption band of **TABO** in 330–400 nm is similar to the lowest-energy absorption band of **TAB**. Our previous study on electroabsorption spectroscopy indicates that the absorption band of **TABO** at around 475 nm is ascribed to the charge transfer transition from the π-orbital of the anthryl group (π(An)) to the vacant p-orbital on the boron atom (p(B)) and, thus, the lowest-energy excited singlet state (S_1^*) is π(An)–p(B) CT in nature [9b]. Contrarily, S_1^* of **TAB** is the locally excited (LE) state (i.e., $\pi\pi^*$ excited state), as judged from the fact that the compound shows the ^1L_a type absorption band as described before. The similarities of the absorption spectrum in 330–400 nm between **TAB** and **TABO** indicate, therefore, that the second excited singlet state (S_2^*) of **TABO** is the LE state. In practice, the electroabsorption spectrum of **TABO** in 330–400 nm has been explained by the LE transition in the anthryl group without any influence of the central boron atom [9b]. These results demonstrate clearly that the presence of the vacant p-orbital on the boron atom in **TABO** plays crucial roles in determining the nature of S_1^* (CT state) and, thus, the spectroscopic and photophysical properties of the molecule. This is in marked contrast to the spectroscopic and photophysical properties of **TAB**.

Reflecting the CT character in S_1^*, **TABO** exhibits broad and structureless fluorescence in 500–650 nm, with Φ^f and τ^f in THF being 0.06 and 4.3 ns, respectively: see Table 4. Although the τ^f value of **TABO** is comparable to that of **TAB** ($\tau^f = 6.8$ ns), the difference in the Φ^f value between **TABO** (0.06) and **TAB** (0.85) is quite large. This brings about very large differences in both k_{nr} and k_f values between the two compounds as the data are included in Table 3. The k_{nr} (=2.2×10^8 s^{-1}) [18] and k_f values (=1.4×10^7 s^{-1}) of **TABO** are 10 times larger and smaller, respectively, than the relevant value of **TAB**: $k_{nr} = 2.2 \times 10^7$ s^{-1} and $k_f = 1.3 \times 10^8$ s^{-1}. The absorption data and Eq. (4) indicate that the k_f^0 value of **TAB** (2.3×10^8 s^{-1}) agrees

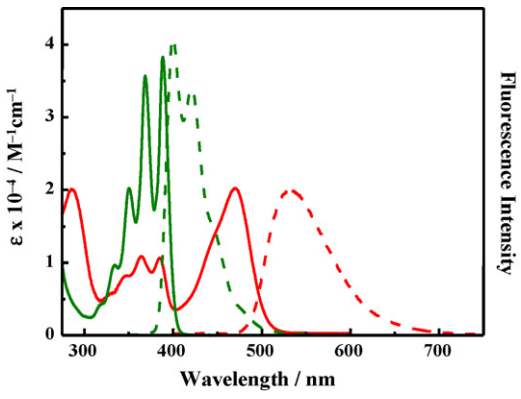

Fig. 5. Absorption (solid curves) and corrected fluorescence spectra (broken curves) of **TAB** (green) and **TABO** (red) in THF at room temperature. (For interpretation of the references to color in this figure legend, the reader is referred to the web version of the article.)

very well with the observed k_f value ($1.3 \times 10^8\ s^{-1}$) as described before, and is also comparable to that of **TABO** ($k_f^0 = 1.5 \times 10^8\ s^{-1}$). Nevertheless, the observed k_f value of **TABO** ($1.4 \times 10^7\ s^{-1}$) was 10 times smaller than k_f^0. As reported previously, S_1^* of **TABO** is degenerated and, light absorption takes place to the allowed excited singlet state, while the fluorescence process is the forbidden transition [9b]. Therefore, the k_f value of **TABO** is observed to be much smaller than that predicted from the absorption data. Such degenerated CT-excited singlet states are observed for various triarylborane derivatives owing to the presence of the vacant p-orbital on the boron atom and D_3 symmetry of the molecule [9,19]. Thus, very weak fluorescence from **TABO** ($\Phi^f = 0.06$) is due essentially to the boron atom connecting three anthryl groups.

It is worth noting that the $\tilde{\mu}$ value of **TAB** is estimated to be 6.4 *D*, while the relevant value ($\Delta\mu$) of **TABO** has been reported to be 8.0 *D* [9]. Owing to CT-excited state nature and $\Delta\mu = 8.0\ D$, the fluorescence characteristics (λ^f, Φ^f, and τ^f) of **TABO** show very large solvent polarity dependences as reported previously [9a]. As an example, a solvent variation from toluene (dielectric constant = 2.38) to CH_3CN (37.5) [20] brings about λ^a and λ^f shifts from 474 to 469 nm and from 521 to 538 nm, respectively. Since **TAB** also possesses a relatively large $\tilde{\mu}$ value ($\sim\Delta\mu$, 6.4 *D*), the λ^a an λ^f values are expected to show solvent polarity dependences. However, **TAB** showed very small λ^a/λ^f shifts; on going from toluene to CH_3CN, λ^a and λ^f were shifted from 390 to 387 nm and from 401 to 397 nm, respectively. The solvent polarity dependence of **TAB** is similar to those of other anthracene derivatives having the lowest-energy LE states [21,22]. Therefore, the solvent dependences of the absorption and fluorescence characteristics of **TAB** and **TABO** will be also explained by the difference in nature of the excited singlet state between **TAB** (LE state) and **TABO** (CT-excited state).

4. Conclusion

Although both **TAB** and **TABO** possess similar propeller-like three-dimensional structures (Scheme 1), the present results demonstrate clearly that the chemical structure of the unit connecting three anthryl groups (phenyl ring or boron atom) plays essential roles in determining the spectroscopic and photophysical characteristics of the compounds. In particular, the presence of the vacant p-orbital on the boron atom in **TABO** influences extraordinary the electronic properties in the excited state, as demonstrated by the characteristic absorption and fluorescence spectra. The benzene ring as the connecting unit for three anthryl groups in **TAB** provides less striking effects on the spectroscopic and photophysical properties of the compound, as compared with the boron atom in **TABO**. Owing to the LE state in nature, however, **TAB** shows intense fluorescence ($\Phi^f = 0.85$), which is marked contrast to weak fluorescence from **TABO** ($\Phi^f = 0.06$). Therefore, the spectroscopic and photophysical characteristics of a triaryl compound can be tuned by the chemical structure of the linkage unit connecting three aryl groups. The CT-excited state of a molecule will be utilized as a fluorescence sensor, while the LE state showing intense fluorescence similar to that of **TAB** is very advantageous for application to a light emitting material. Such functional molecular materials could be designed by an appropriate choice of the chemical structure connecting multi-π-electron chromophores.

Acknowledgements

This work was supported by Grant-in-Aids for Science Research on Priority Research Areas (Nos. 19027002 and 20036002, Synergy Elements) from the Ministry of Education, Culture, Sports, Science, and Technology, Japan. E. S. acknowledges Japan Society for the Promotion of Science for a research fellowship for young scientists.

References

[1] J.B. Birks, Photophysics of Aromatic Molecules, Wiley-Interscience, London, 1970.
[2] J.B. Birks (Ed.), Molecular Organic Photophysics, vol. I, John Wiley & Sons, London, 1973;
J.B. Birks (Ed.), Molecular Organic Photophysics, vol. II, John Wiley & Sons, London, 1975.
[3] M. Montalti, A. Credi, L. Prodi, M.T. Gandolfi, Handbook of Photochemistry, 3rd ed., Taylor & Francis, Boca Raton, 2006.
[4] (a) N. Mataga, H. Yao, T. Okada, W. Rettig, J. Phys. Chem. 93 (1989) 3383;
(b) N. Mataga, S. Nishikawa, T. Okada, Chem. Phys. Lett. 257 (1996) 327;
(c) T. Fujiwara, Y. Fujimura, O. Kajimoto, J. Chem. Phys. 113 (2000) 11109;
(d) M. Jurczok, P. Plaza, M.M. Martin, Y.H. Meyer, W. Rettig, Chem. Phys. 253 (2000) 339;
(e) Z.R. Grabowski, K. Rotkiewicz, W. Rettig, Chem. Rev. 103 (2003) 3899;
(f) T. Takaya, S. Saha, H. Hamaguchi, M. Sarkar, A. Samanta, K. Iwata, J. Phys. Chem. A 110 (2006) 4291;
(g) G.-J. Zhao, Y.-H. Liu, K.-L. Han, Y. Dou, Chem. Phys. Lett. 453 (2008) 29.
[5] (a) T. Okada, N. Mataga, W. Baumann, A. Siemiarczuk, J. Phys. Chem. 91 (1987) 4490;
(b) V. Nagarajan, A.M. Brearley, T.-J. Kang, P.F. Barbara, J. Chem. Phys. 86 (1987) 3183;
(c) N. Mataga, S. Nishikawa, T. Asahi, T. Okada, J. Phys. Chem. 94 (1990) 1443;
(d) D. Bandyopadhyay, D. Majumdar, K.K. Das, J. Mol. Struct. 389 (1997) 179;
(e) M.M. Martin, P. Plaza, P. Changenet-Barret, A. Siemiarczuk, J. Phys. Chem. 106 (2002) 2351.
[6] K. Suzuki, A. Seno, H. Tanabe, K. Ueno, Synth. Met. 143 (2004) 89.
[7] (a) S. Yamaguchi, S. Akiyama, K. Tamao, J. Am. Chem. Soc. 122 (2000) 6335;
(b) S. Yamaguchi, S. Akiyama, K. Tamao, J. Am. Chem. Soc. 123 (2001) 11372;
(c) S. Yamaguchi, S. Akiyama, K. Tamao, J. Organomet. Chem. 652 (2002) 3.
[8] E. Sakuda, K. Tsuge, Y. Sasaki, N. Kitamura, J. Phys. Chem. B 109 (2005) 22326.
[9] (a) N. Kitamura, E. Sakuda, J. Phys. Chem. A 109 (2005) 7429;
(b) N. Kitamura, E. Sakuda, T. Yoshizawa, T. Iimori, N. Ohta, J. Phys. Chem. A 109 (2005) 7435.
[10] X.-F. Wang, X.-R. Zhang, Y.-S. Wu, J.-P. Zhan, X.-C. Ai, Y. Wang, M.T. Sun, Chem. Phys. Lett. 436 (2007) 280.
[11] (a) L. Brauge, G. Vériot, G. Franc, R. Deloncle, A.-M. Caminade, J.-P. Majoral, Tetrahedron 62 (2006) 11891;
(b) S. Tao, S. Xu, X. Zhang, Chem. Phys. Lett. 429 (2006) 622;
(c) S.-K. Kim, Y.-I. Park, I.-N. Kang, J.-W. Park, J. Mater. Chem. 17 (2007) 4670;
(d) T. Karatsu, R. Hazuku, M. Asuke, A. Nishigaki, S. Yagai, Y. Suzuri, H. Kita, A. Kitamura, Org. Electron. 8 (2007) 357.
[12] (a) S.-M. Cheung, W.-H. Chan, Tetrahedron 62 (2006) 8379;
(b) Z. Xu, S. Kim, K.-H. Lee, J. Yoon, Tetrahedron Lett. 48 (2007) 3797;
(c) G. Zhang, G. Yang, S. Wang, Q. Chen, J.S. Ma, Chem. Eur. J. 13 (2007) 3630;
(d) J. Kim, T. Morozumi, H. Nakamura, Org. Lett. 9 (2007) 4419.
[13] M. Takahashi, H. Morimoto, K. Miyake, H. Kawai, Y. Sei, K. Yamaguchi, T. Sengoku, H. Yoda, New J. Chem. 32 (2008) 547.
[14] (a) C.M. Whitaker, R.J. MaMohon, J. Phys. Chem. 100 (1976) 1081;
(b) M. Baumgarten, L. Gherghel, J. Friedrich, M. Juurczok, W. Rettig, J. Phys. Chem. A 104 (2000) 1130;
(c) Z.H. Li, M.S. Wong, Y. Tao, M. D'Iorio, J. Org. Chem. 69 (2004) 921.
[15] J.V. Morris, M.A. Mahaney, J.R. Huber, J. Phys. Chem. 80 (1976) 969.
[16] H.-B. Kim, S. Habuchi, N. Kitamura, Anal. Chem. 71 (1999) 842.
[17] (a) H.K. Sinha, K. Yates, J. Chem. Phys. 93 (1990) 7085;
(b) S. Muralidharan, H.K. Sinha, K. Yates, J. Phys. Chem. 95 (1991) 8517.
[18] The major nonradiative decay path from the CT-excited singlet state of TABO is internal conversion to the ground state as revealed by the energy gap dependence of the $\ln k_{nr}$ value [9a].
[19] (a) B.G. Ramsey, M. El-Bayoumi, M. Kasha, J. Phys. Chem. 35 (1961) 1502;
(b) B.G. Ramsey, J.E. Leffler, J. Phys. Chem. 67 (1963) 2242;
(c) B.G. Ramsey, J. Phys. Chem. 70 (1966) 611.
[20] Organic solvent, in: J.A. Riddick, W.B. Bunger (Eds.), in: Techniques of Chemistry, vol. II, 3rd ed., Wiley-Interscience, New York, 1970.
[21] P. Suppan, N. Ghoneim, Solvatochromism, The Royal Society of Chemistry, Cambridge, 1997.
[22] N. Ghoneim, P. Suppan, Spectrochim. Acta 51A (1995) 1043.